Scientific Research Publishing

Graphene, 2026, 15(1), 1-17
https://www.scirp.org/journal/graphene
ISSN Online: 2169-3471
ISSN Print: 2169-3439

Emergent Magnetism and Symmetry Breaking in Half-Functionalized Silicene from First Principles

N'goyé Bré-Junior Kanga[1,2], Boris Irie Bi[1], N'Gbesso Josée Yao[1], Aboudrame Kone[1], Lalla Btissam Drissi[2], Raymond N'Guessan Kre[3]

[1]Department of Physics, University of Man, Man, Côte d'Ivoire
[2]CPM, Centre of Physics and Mathematics-Morocco, Faculty of Science, Mohammed V University, Rabat, Morocco
[3]Faculty of Fundamental and Applied Sciences, Nangui Abrogoua University, Abidjan, Côte d'Ivoire
Email: junior.kanga@univ-man.edu.ci

How to cite this paper: Kanga, N.B.-J., Bi, B.I., Yao, N.J., Kone, A., Drissi, L.B. and Kre, R.N. (2026) Emergent Magnetism and Symmetry Breaking in Half-Functionalized Silicene from First Principles. *Graphene*, **15**, 1-17.
https://doi.org/10.4236/graphene.2026.151001

Received: October 8, 2025
Accepted: January 28, 2026
Published: January 31, 2026

Abstract

The ability to dynamically tune the electronic and magnetic phases of two-dimensional materials is a critical prerequisite for advanced spintronic applications. In this study, we perform first-principles density functional theory (DFT) calculations, utilizing Projector Augmented-Wave (PAW) pseudopotentials, to investigate the structural, electronic, and magnetic properties of half-hydrogenated and half-fluorinated silicene monolayers. Our energetic and structural analyses reveal that single-sided adatom chemisorption selectively breaks the intrinsic sublattice symmetry, inducing significant out-of-plane charge transfer while maintaining the covalent integrity of the underlying silicon framework. Consequently, the pristine zero-gap Dirac semimetal is fundamentally transformed. Indeed, half-hydrogenation yields an indirect-gap semiconductor, whereas half-fluorination results in an indirect-gap semimetal. Crucially, this site-selective functionalization isolates unpaired electrons on the unpassivated silicon sublattices, driving macroscopic magnetic ordering. Spin-polarized calculations determine that the half-hydrogenated configuration stabilizes in a ferromagnetic ground state with a Curie temperature of T_C = 30.6 K, driven by the unpassivated Si *p*-orbitals. Conversely, the half-fluorinated configuration exhibits an antiferromagnetic ground state governed by a collective electronic contribution from both the unpassivated Si and adatom F *p*-orbitals. These findings establish half-functionalization as a highly effective, non-destructive strategy to engineer symmetry-broken magnetic phases in silicene, offering a tunable platform for silicon-compatible cryogenic spintronics and nanoscale logic devices.

Keywords

Silicene, Half-Functionalization, Density Functional Theory (DFT), Spintronics, Ferromagnetism, Antiferromagnetism, Electronic Band Structure

1. Introduction

Following the experimental realization of graphene and the subsequent observation of its extraordinary physical properties [1], two-dimensional (2D) materials have emerged as a dominant paradigm in condensed matter physics. The remarkable ultrahigh carrier mobility, thermal conductivity, and mechanical strength of graphene have established a blueprint for nanoscale technological applications [2]. Driven by this potential, extensive research has shifted toward other group-IV monolayers—namely, silicene [3], germanene [4], and stanene [5]. Unlike graphene, the buckled atomic structures of these silicene-like materials provide an ideal platform for surface functionalization, unlocking a vast landscape of tunable electronic and phononic properties [6].

Owing to their analogous honeycomb lattices, these 2D materials share several fascinating properties with graphene, most notably a Dirac-like electronic band structure near the Fermi level [7]. Consequently, they exhibit high carrier mobility [3] [4], excellent mechanical flexibility, and remarkable electronic transport characteristics, making them highly promising candidates for nanoelectronic applications. Furthermore, the heavier elemental composition of germanene and stanene induces significantly stronger spin-orbit coupling compared to graphene [5]. This intrinsic feature provides new opportunities for tuning their electronic and magnetic properties, paving the way for advanced spintronic devices [8].

Despite these advantageous characteristics, the absence of an intrinsic band gap and long-range magnetic order in pristine group-IV monolayers severely hinders their integration into functional electronic, optoelectronic, and spintronic devices. To overcome these inherent limitations, extensive research has focused on tailoring their band structures and magnetic responses. Recent experimental breakthroughs have demonstrated that coupling silicene with rare-earth metals (such as Eu or Gd) can induce complex, competing magnetic orders, driving a transition from 3D antiferromagnetism to 2D ferromagnetism [9]. Among the various modification strategies, surface passivation via chemical functionalization, specifically through hydrogenation and fluorination, has emerged as a highly effective approach to engineer these fundamental properties [10]-[12].

When functionalizing the basal plane of these monolayers, a distinct trade-off emerges between energetic viability and functional utility. Computations consistently reveal that fluorine termination produces a deeper thermodynamic minimum compared to hydrogen adsorption [11] [13]. Despite this relative energetic disadvantage, modifying the lattice with hydrogen remains a dominant research

avenue. Its unique ability to alter orbital hybridization in a way that triggers magnetic ordering and sculpts the electronic band gap makes it an indispensable tool for developing nanoscale spintronic architectures.

The successful experimental realization of silicane, the fully hydrogenated analog of silicene, represents a major milestone in the development of functionalized group-IV monolayers [14]. Structurally, this derivative features a buckled hexagonal silicium lattice where each host atom is covalently passivated by a hydrogen adatom, ensuring robust structural stability. Much like graphane [11], this saturated framework exhibits highly desirable electronic traits, most notably excellent carrier mobility and the emergence of a finite band gap, positioning it as a prime candidate for next-generation nanoelectronics and spintronics. Crucially, diffuse reflectance absorption spectroscopy has confirmed an optical band gap of approximately 2.94 eV [15], firmly establishing silicane as a viable 2D semiconductor.

While full hydrogenation thus offers an effective route toward a sizeable and robust band gap, the resulting silicane remains non-magnetic, since the complete saturation of every silicon atom quenches the unpaired p_z electrons that would otherwise sustain spin polarization [16]. Achieving simultaneous control over both the electronic band gap and the magnetic ordering therefore calls for only partial saturation of the lattice, whereby a fraction of the host atoms remains chemically unsaturated and retains localized, unpaired electrons capable of inducing magnetism. In this work, we explore this strategy by investigating two partial functionalization routes, half-hydrogenation and half-fluorination of the silicene monolayer, and demonstrate that they give rise to fundamentally different electronic and magnetic ground states. The hydrogenated structure stabilizes a ferromagnetic order with a sizeable band gap of 0.92 eV, whereas the fluorinated structure favors an antiferromagnetic order with semi-metallic behavior. The negative formation energies obtained for both configurations confirm their thermodynamic stability, underscoring their potential as versatile, silicon-based platforms for next-generation spintronic and nanoelectronic applications.

The rest of this article proceeds as follows. Section 2 establishes the first-principles methodology used to model our systems. Section 3 presents our core results, discussing how targeted chemical functionalization governs the structural stability, band gap evolution, and magnetic ordering of the silicene monolayers. We present our final conclusions in Section 4.

2. Computational Methods

All calculations were performed within the framework of Density Functional Theory (DFT) [17] using the Quantum ESPRESSO package [18], where the Kohn-Sham equations were solved self-consistently [19]. Exchange-correlation effects were described by the Perdew-Burke-Ernzerhof (PBE) functional within the Generalized Gradient Approximation (GGA) [20]. To properly account for the long-range dispersion interactions characteristic of two-dimensional systems, van der Waals effects were included through the nonlocal vdW-DF2 functional [21] [22], based

on the nonlocal correlation formalism developed by the Thonhauser group [21] [22]. Specifically, the PBE functional augmented with the vdW-DF2 correction was applied consistently across all stages of the workflow, including structural relaxation, total energy evaluation, and electronic band structure generation. The interaction between valence electrons and ionic cores was treated using the Projector Augmented-Wave (PAW) method [23]. The computational parameters were carefully converged with respect to the plane-wave cutoff energy, charge-density cutoff, k-point sampling, and lattice parameter. The electronic wave functions were expanded in a plane-wave basis set with a kinetic energy cutoff of 65 Ry, while a charge-density cutoff of 360 Ry was employed. Brillouin-zone integrations were carried out using a $60 \times 60 \times 1$ Monkhorst-Pack k-point mesh, which ensured the convergence of the total energy and electronic properties. To eliminate spurious interactions between periodically repeated images, a vacuum region larger than 18 Å was introduced along the direction perpendicular to the monolayer plane. The structural optimization was carried out in a two-step procedure to ensure high accuracy. First, a variable-cell relaxation was performed to optimize the in-plane lattice parameters while constraining the out-of-plane axis to preserve the 18 Å vacuum gap. Subsequently, a standard relaxation at the fixed optimized cell dimensions was conducted to precisely determine the internal atomic coordinates. For both steps, the relaxation was considered complete when the total energy change between self-consistent steps dropped below 10^{-8} Ry, and the maximum Hellmann-Feynman force acting on any atom was reduced to less than 10^{-4} Ry/Bohr.

3. Results and Discussion

3.1. Energetic Stability

To rigorously assess the thermodynamic viability of the functionalized silicene configurations, both the binding energy (E_B) and the formation energy (E_f) were calculated for the respective hydrogen and fluorine chemisorption processes. The binding energy serves as a quantitative measure of the overall interaction strength, encompassing both the newly formed adatom bonds (Si-H or Si-F) and the intrinsic Si-Si lattice. Consequently, a larger absolute magnitude of E_B signifies more robust structural cohesion. This energetic metric is formally expressed as [24]:

$$E_B = \frac{1}{N}\left(E_T - E_{Si} - n_X E_X\right),$$

where N denotes the total number of atoms comprising the supercell, and E_T represents the calculated total energy of the functionalized (hydrogenated or fluorinated) system. The term E_{Si} corresponds to the total energy of the pristine silicene monolayer. Furthermore, E_X defines the energy of an isolated adatom (X = H or F), while n_X indicates the exact number of these specific adatoms adsorbed onto the lattice.

In parallel, the formation energy (E_f) evaluates the thermodynamic stability of the functionalized lattice relative to its molecular gas phase, effectively quantifying

the system's resistance against the desorption of diatomic H_2 or F_2 molecules. This energetic parameter is defined by the following relation [24]:

$$E_f = \frac{1}{N}\left(E_T - E_{\mathrm{Si}} - \frac{n_{\mathrm{X}}}{2}E_{\mathrm{X}_2}\right),$$

where E_{X_2} denotes the calculated total energy of an isolated reference molecule (H_2 or F_2). A strictly negative value for E_f indicates that the chemisorption process is exothermic. This thermodynamic favorability indicates that the half-functionalized configurations are energetically stable against phase decomposition. However, we note that definitive proof of experimental viability would also necessitate confirming their dynamical and thermal stability, which remains a compelling subject for future investigations.

The calculated formation and binding energies for both half-functionalized configurations are strictly negative, confirming that the adatom chemisorption is an inherently exothermic process and that the resulting monolayers are thermodynamically stable. Notably, the half-hydrogenated configuration exhibits a significantly larger absolute binding energy (E_B). This indicates that hydrogen passivation of the silicon lattice yields a more energetically favorable ground state compared to fluorine adsorption, providing a robust physical rationale for the extensive focus on hydrogenation in prior studies of 2D materials. Quantitatively, the formation and binding energies between the two functionalized hybrids exhibit energetic differences of 0.13 eV/atom and 0.53 eV/atom, respectively. Ultimately, both thermodynamic metrics consistently favor the half-hydrogenated silicene lattice, definitively establishing its enhanced energetic stability relative to its half-fluorinated counterpart.

3.2. Structural Properties

Silicene differs fundamentally from graphene through its intrinsic buckled geometry, which originates from the larger atomic radius of silicon and its mixed sp^2-sp^3 hybridization character [25]. The resulting vertical displacement between the two hexagonal sublattices breaks the planar symmetry and creates chemically inequivalent adsorption environments. Such a buckled structure is particularly favorable for sublattice-selective functionalization, enabling the formation of semi-functionalized derivatives through the adsorption of adatoms on a single sublattice. In this work, two configurations are considered: semi-hydrogenated silicene, where hydrogen atoms are attached to one silicon sublattice (**Figure 1(a)**), and semi-fluorinated silicene, obtained by the adsorption of fluorine atoms on the same sublattice (**Figure 1(b)**).

The optimized structural parameters of the half-functionalized silicene configurations are summarized in **Table 1**. Compared with pristine silicene [26], both functionalized structures exhibit elongated Si-Si bonds, indicating that adatom adsorption induces a noticeable reconstruction of the silicon lattice. For the half-hydrogenated configuration, the calculated Si-Si bond length and buckling height are 2.375 Å and 0.6802 Å, respectively. The half-fluorinated structure exhibits a

slightly shorter Si-Si bond length of 2.367 Å, while retaining a nearly identical buckling height of 0.6804 Å. The remarkable similarity of the buckling parameters suggests that the adsorption of either hydrogen or fluorine drives the silicon atoms from their mixed sp^2/sp^3 hybridization toward a predominantly sp^3-like tetrahedral environment. As a result, the out-of-plane distortion is primarily dictated by the geometrical constraints associated with sp^3 bonding rather than by the different electronegativities of the adsorbed species. The calculated adatom-silicon bond lengths are 1.507 Å for the Si-H bond and 1.649 Å for the Si-F bond, reflecting the larger atomic size of fluorine and the distinct bonding characteristics of the two adatoms.

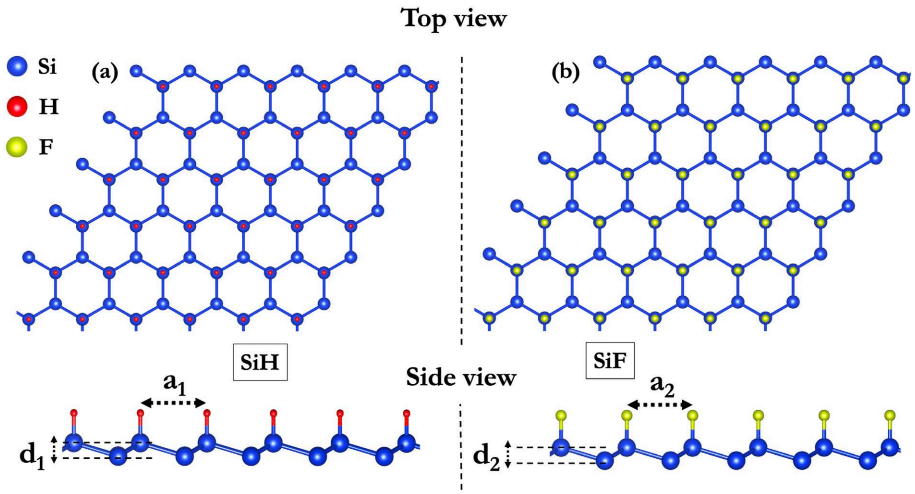

Figure 1. Optimized atomic structures of the half-functionalized silicene monolayers. The blue, red, and yellow spheres represent silicon (Si), hydrogen (H), and fluorine (F) atoms, respectively. Top and side views are shown for the (a) half-hydrogenated and (b) half-fluorinated configurations. The parameters a_1 and a_2 denote the lattice constants, while d_1 and d_2 represent the out-of-plane buckling distances for the hydrogenated and fluorinated structures, respectively.

Table 1. Calculated results for semi-functionalized silicene: Distances and buckling parameter Δ in Å, formation E_f, binding E_B, and gap energies E_g in eV.

Structures	d_{Si-Si}	d_{H-Si}	d_{F-Si}	Δ	E_B	E_f	E_g	Magnetism
Hydrogenated	2.375	1.507	-	0.68	−2.76	−2.61	0.92	FM
Fluorinated	2.367	-	1.649	0.68	−2.23	−2.48	-	AFM

3.3. Charge Transfer

To elucidate the nature of the chemical bonding and electronic interactions within the half-functionalized silicene configurations, Figure 2 illustrates the spatial charge density distributions. In both systems, a pronounced localization of electronic charge is observed around the adatoms, accompanied by a corresponding charge depletion surrounding the host silicon atoms. Specifically, the electron density is concentrated both around the adatoms and along the adatom—Si axis,

indicating a strongly polar covalent bonding character. This charge transfer is fundamentally driven by the Pauling electronegativity (χ) differences between the constituent elements [27]. As depicted in the side views of **Figure 2(a)** and **Figure 2(b)**, the charge accumulation is significantly more prominent around the fluorine atom (χ = 3.98) than the hydrogen atom (χ = 2.20), which perfectly aligns with their relative electronegativities compared to silicon (χ = 2.01). Finally, an analysis of the charge distribution between the passivated silicon and the adjacent free silicon reveals that the electron density remains symmetrically localized between the two atoms, confirming that the underlying Si-Si lattice strongly retains its intrinsic covalent bonding character.

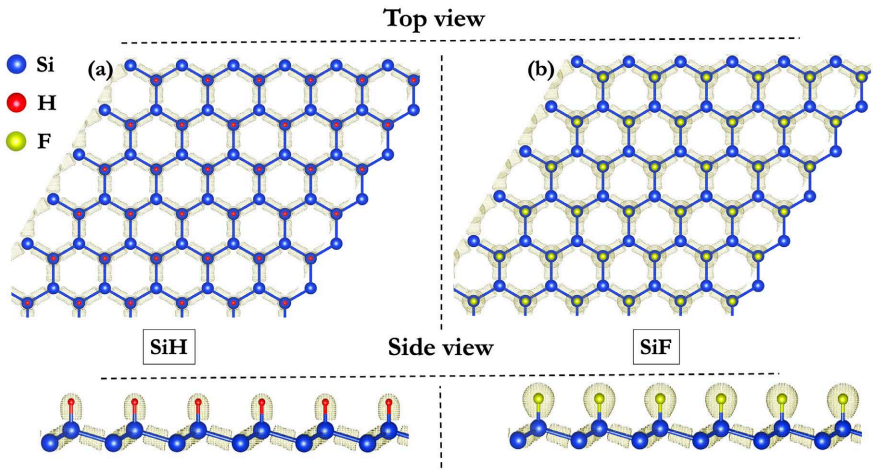

Figure 2. Charge density distribution of the half-functionalized silicene monolayers. The blue, red, and yellow spheres represent silicon (Si), hydrogen (H), and fluorine (F) atoms, respectively. Top and side views are shown for the (a) half-hydrogenated and (b) half-fluorinated configurations.

To quantitatively substantiate the polarizations observed in the charge density maps in **Figure 2**, a Bader charge analysis [28] was performed, with the results summarized in **Table 2**. Consistent with the previously discussed electronegativity differences, we observe an electron transfer from the passivated silicon atoms to the adatoms. Specifically, the hydrogen-bonded silicon atoms donate approximately 0.97 e− to the hydrogen atoms. In the half-fluorinated configuration, the extreme electronegativity of fluorine drives an even greater charge transfer, with the functionalized silicon donating nearly 1.006 e− to the F atom. These local redistributions confirm the strong mixed ionic-covalent character of the Si-H and Si-F bonds. Despite this severe vertical polarization, the charge transfer along the in-plane silicene lattice remains remarkably small. Specifically, the unpassivated, free Si atoms receive only 0.023 e− and 0.0017 e− per adjacent Si-Si bond from their functionalized neighbors in the hydrogenated and fluorinated structures, respectively. Because each free Si atom bonds to three functionalized neighbors, this results in a total net charge accumulation of approximately 0.07 e− and 0.005 e− per unpassivated atom, which perfectly aligns with the total Bader charges reported

in Table 2. This negligible in-plane charge transfer definitively proves that the underlying Si-Si network strongly preserves its purely covalent bonding character.

Table 2. Calculated charge transfer for the two semi-functionalized silicene configurations. The symbols "+" and "−" indicate electron accumulation and electron depletion, respectively.

Structures	*Si*	$Si_{/H}$	$Si_{/F}$	*H*	*F*
Hydrogenated	+0.07	−1.04	-	+0.97	-
Fluorinated	+0.005	-	−1.02	-	+1.006

3.4. Electronic Structure

Given that the fundamental electronic properties of pristine silicene have been extensively documented in existing literature, this study bypasses its baseline characterization. Instead, our analysis is strictly devoted to the half-functionalized configurations to systematically evaluate how hydrogen and fluorine adsorption modulate the electronic topology of the monolayer. The computed electronic band structures for both systems are depicted in Figure 3, while the extracted band-gap values are tabulated in Table 1.

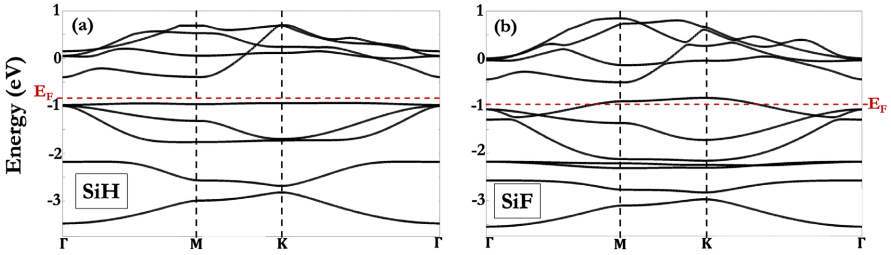

Figure 3. The electronic band structure for half-functionalized silicene configurations: (a) half-hydrogenated and (b) half-fluorinated configurations.

Pristine freestanding silicene is well known to exhibit a semi-metallic character, featuring Dirac-like band crossings at the Fermi level that result in a zero band gap [5] [11]. While the inclusion of spin-orbit coupling can induce a negligible gap in the pristine sheet [29], our results demonstrate that chemical functionalization fundamentally alters this electronic topology. As depicted in Figure 3, a substantial, finite band gap is opened for both the half-hydrogenated and half-fluorinated configurations even in the absence of spin-orbit interactions. This dramatic transition from a Dirac semimetal to a gapped system underscores the powerful influence of targeted adatom adsorption in breaking the sublattice symmetry of the silicene monolayer.

As illustrated in Figure 3(a), the half-hydrogenated configuration exhibits a calculated band gap of approximately E_g = 0.92 eV, whereas the half-fluorinated structure (Figure 3(b)) exhibits a semi-metallic character. Beyond this variance in gap magnitude, the choice of adatom fundamentally dictates the resulting elec-

tronic topology. Both passivated systems display an indirect band-gap profile, characterized by a conduction band minimum (CBM) located near the M point and a valence band maximum (VBM) situated at the K point. However, a distinct divergence in electronic behavior emerges in the half-fluorinated system: the partial occupation of valence states causes the bands to cross the Fermi level, thereby imparting a semi-metallic character. Ultimately, these findings highlight that chemical passivation does more than simply break the zero-gap state of pristine silicene; it serves as a powerful mechanism to tune the overall electronic phase, driving the material to behave either as an indirect semiconductor or a semi-metal depending on the functionalizing agent.

To elucidate the orbital contributions along the high-symmetry directions of the Brillouin zone, the projected electronic band structures for the half-functionalized configurations are presented in Figure 4. For the half-hydrogenated system (Figure 4(a)), the states near the valence band maximum (VBM) are predominantly derived from the $3p_y$ orbitals of the unpassivated silicon atoms, accompanied by a minor contribution from the hydrogen $1s$ orbitals. These Si $3p_y$ states remain the dominant component across most of the high-symmetry pathway near the VBM. Conversely, the conduction band minimum (CBM) originates largely from the $3s$ orbitals of the free silicon atoms, although the hydrogen $1s$ states contribute notably in the vicinity of the K-point. Collectively, these observations demonstrate that the electronic states bordering the Fermi level are fundamentally governed by the unpassivated silicon lattice, whereas the passivated silicon atoms exert only a negligible influence near the band edges.

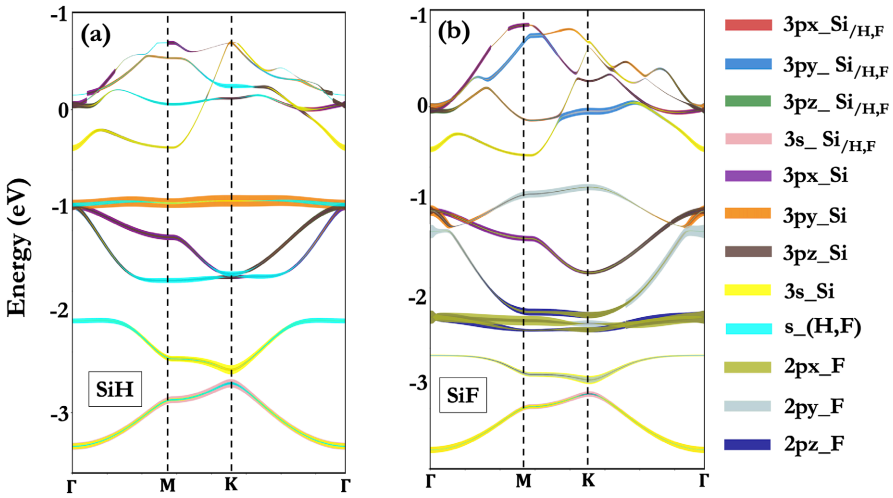

Figure 4. Orbital-projected electronic band structures of the half-functionalized silicene configurations: (a) the half-hydrogenated system and (b) the half-fluorinated system.

For the half-fluorinated configuration displayed in Figure 4(b), a similar orbital distribution is observed near the valence-band edge. The VBM is mainly dominated by the p_y orbitals of the adsorbed fluorine (F) atoms, particularly on the M-K path of the high symmetry line of the Brillouin zone. This contribution is fol-

lowed by the contribution of $3p_y$ orbitals of the Si atom which is not bonded to the fluorine atom. The conduction band minimum (CBM) receives an important contribution from the non-bonded to the fluorine silicon Si atoms $3s$ orbitals, especially on the Γ-M, from the M point to the middle of the M-K path and from the middle of the K-Γ to Γ point. The $3p_y$ orbitals of Si not bonded to fluorine dominate the CBM over all this previous domain of the high symmetry line of the Brillouin zone. At the CBM, around the K-point, $3p_y$ orbitals of the fluorine-bonded silicon $Si_{/F}$ is the dominant one. Overall, the projected band structure analysis reveals that the electronic states around the Fermi level do not arise from only one or two orbitals but arise from a mixed contribution of all atoms present in the structure; however, the dominant one is the $2p_y$ orbitals of the adsorbed fluorine F atoms.

On the other hand, for the half-fluorinated configuration (**Figure 4(b)**), a highly hybridized orbital distribution emerges near the Fermi level. The valence band maximum (VBM) is heavily dominated by the $2p_y$ orbitals of the adsorbed fluorine atoms, particularly along the M-K high-symmetry path, with secondary contributions arising from the $3p_y$ orbitals of the unpassivated silicon atoms. In the conduction band region, the orbital character exhibits strong momentum dependence. Along the Γ-M direction and the path segments radiating from both the Γ and M points, the conduction band minimum (CBM) is primarily governed by the $3p_y$ orbitals of the free silicon atoms, supplemented by a notable contribution from their $3s$ states. However, as the momentum approaches the K point, the CBM character shifts abruptly, becoming dominated by the $3p_y$ orbitals of the passivated (fluorine-bonded) silicon atoms. Ultimately, this analysis reveals that the electronic states bordering the Fermi level are not isolated to a single atomic site; rather, they arise from a complex hybridization among all atoms in the lattice, with the strongly electronegative fluorine $2p_y$ states acting as the paramount driving force.

3.5. Magnetic Properties

The chemical functionalization of the silicene monolayer fundamentally disrupts its extended π-bonding network. By passivating only half of the lattice, localized unpaired electrons are generated on the remaining unpassivated silicon atoms, providing a physical mechanism for emergent magnetic ordering. To rigorously determine the magnetic ground state of both the half-hydrogenated and half-fluorinated configurations, spin-polarized calculations were performed within the GGA framework. We evaluated three distinct magnetic arrangements: non-magnetic (NM), ferromagnetic (FM), and antiferromagnetic (AFM). As depicted in **Figure 6**, the magnetic phases were modeled using a $4 \times 4 \times 1$ supercell comprising 48 atoms per configuration (32 silicon atoms and 16 adatoms). To ensure computational accuracy, the initial spin polarizations during the self-consistent cycles were specifically localized on the 16 unpassivated silicon atoms, as they are the primary hosts for the induced magnetic moments.

An analysis of the calculated total energies reveals that the choice of adatom

fundamentally dictates the magnetic ground state of the functionalized monolayer. For the half-hydrogenated configuration, the ferromagnetic (FM) state is energetically most stable compared to both the antiferromagnetic (AFM) and non-magnetic (NM) phases. Conversely, energy minimization establishes the AFM state as the definitive ground state for the half-fluorinated system. To quantitatively substantiate the assigned magnetic ground states, the total energies of the NM, FM, and AFM configurations were systematically evaluated and compared. For the half-hydrogenated system, the FM state is energetically the most stable, lying 63.28 meV per supercell lower than the AFM state and 44.71 meV per supercell lower than the NM state. Conversely, for the half-fluorinated system, the AFM phase constitutes the definitive ground state, being energetically favored by 24.88 meV per supercell over the FM state and 47.42 meV per supercell over the NM state. To quantify the spin polarization in the FM half-hydrogenated structure, a Löwdin population analysis [30] was performed. The results indicate that the passivated silicon atoms and the hydrogen adatoms exhibit negligible magnetic moments of approximately 0.0070 μ_B and 0.1085 μ_B, respectively. Instead, the robust macroscopic magnetization is overwhelmingly driven by the unpassivated silicon atoms, which host a highly localized magnetic moment of about 0.8703 μ_B per atom. In the AFM half-fluorinated structure, the local magnetic moments on the unpassivated silicon sublattices align in an antiparallel configuration, yielding a net macroscopic magnetic moment of absolute zero for the supercell. Ultimately, these results demonstrate that, while both functionalizations induce localized spins, half-hydrogenation is specifically required to stabilize long-range ferromagnetic ordering in silicene.

While half-hydrogenation successfully induces a ferromagnetic ground state, the relatively narrow energy difference between the FM and AFM configurations implies that this magnetic ordering is highly susceptible to thermal fluctuations. To evaluate the Curie temperature (T_C), the exchange coupling parameter (J) was extracted by mapping the DFT total energies onto the classical nearest-neighbor Heisenberg spin model, defined as:

$$H = -J\sum_{i,j}\mathbf{S}_i \cdot \mathbf{S}_j.$$

By comparing the energies of the ferromagnetic and antiferromagnetic states, the exchange parameter is derived using the mapping formula:

$$J = \frac{E_{AFM} - E_{FM}}{zS^2},$$

where z is the effective coordination number and $S = 1/2$ is the spin magnitude per site. From this, the Curie temperature within the Mean Field Approximation (MFA) can be estimated using the global relation:

$$T_C = \frac{2\left(E_{AFM} - E_{FM}\right)}{3Nk_B},$$

where N is the total number of magnetic atoms in the supercell, and k_B is the

Boltzmann constant. Using the calculated exchange energy of approximately 3.95 meV per magnetic atom (derived from the 63.28 meV energy difference across the 16 unpassivated silicon atoms in our supercell), we obtain an estimated T_C of 30.6 K. It is important to note, however, that while the MFA provides a useful qualitative baseline, it intrinsically neglects long-range thermal spin fluctuations. In two-dimensional systems, these fluctuations are highly pronounced (as dictated by the Mermin-Wagner theorem), meaning the MFA fundamentally overestimates the true ordering temperature, which relies on magnetic anisotropy to maintain long-range order. This result reveals that while robust long-range ferromagnetic order is intrinsically stabilized by hydrogen passivation, it is strictly maintained only in the low-temperature regime, restricting potential spintronic applications to cryogenic environments.

To further validate the assigned magnetic ground states and gain deeper insight into the underlying electronic exchange mechanisms, spin-polarized electronic band structures were calculated for both configurations, as presented in **Figure 5**. For the half-hydrogenated system (**Figure 5(a)**), a pronounced exchange splitting between the spin-up (majority) and spin-down (minority) channels is highly visible across the entire Brillouin zone. This macroscopic band asymmetry perfectly aligns with the localized spin polarization discussed previously, providing definitive confirmation of the robust ferromagnetic character intrinsic to the half-hydrogenated silicene lattice.

In stark contrast, the half-fluorinated configuration (**Figure 5(b)**) exhibits a fundamentally different electronic topology. Unlike the pronounced exchange splitting observed in the hydrogenated system, the spin-up and spin-down energy bands of the fluorinated monolayer are perfectly degenerate across the entire Brillouin zone. This complete energetic overlap of the majority and minority spin channels indicates an absence of macroscopic spin polarization. Such continuous spin degeneracy is a quintessential hallmark of a system with zero net magnetization, thereby providing definitive confirmation of the antiferromagnetic ground state, wherein the localized magnetic moments on the unpassivated silicon sublattices perfectly cancel each other out.

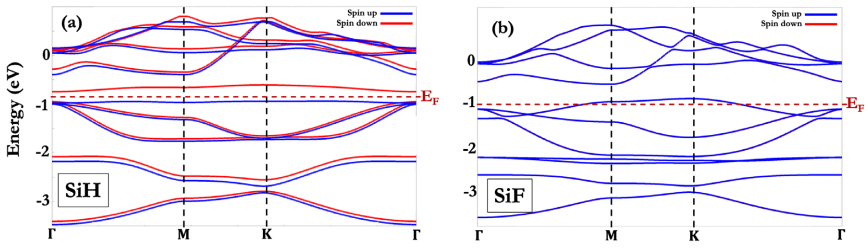

Figure 5. Spin-polarized electronic band structures of the half-functionalized silicene configurations. (a) The half-hydrogenated system exhibits pronounced exchange splitting between the majority and minority spin channels, indicative of ferromagnetic ordering. (b) The half-fluorinated system displays perfectly degenerate spin bands, characteristic of an antiferromagnetic ground state.

To further visualize the macroscopic magnetic behavior of the functionalized monolayers, the spatial spin-density distributions ($\Delta\rho$) for both configurations are plotted in Figure 6. In both systems, the spin-density isosurfaces are overwhelmingly localized on the unpassivated silicon atoms, visually corroborating our previous analyses that these sites are the primary hosts of the induced magnetic moments. Conversely, the passivated silicon atoms and their respective adatoms exhibit negligible spin density, confirming their minimal contribution to the overall magnetization. The stark contrast between the two magnetic ground states becomes explicitly apparent when examining the spatial alignment of these localized lobes. For the half-hydrogenated configuration (Figure 6(a)), the spin-density isosurfaces display a uniform spatial phase (identical coloration) across all magnetic sites, visually confirming the parallel spin alignment characteristic of robust ferromagnetic ordering. In contrast, the half-fluorinated configuration (Figure 6(b)) exhibits alternating regions of positive and negative spin density on adjacent unpassivated silicon atoms. This antiparallel spatial distribution flawlessly visualizes the localized spin cancellation, providing a compelling final confirmation of the antiferromagnetic ground state predicted by the total-energy calculations.

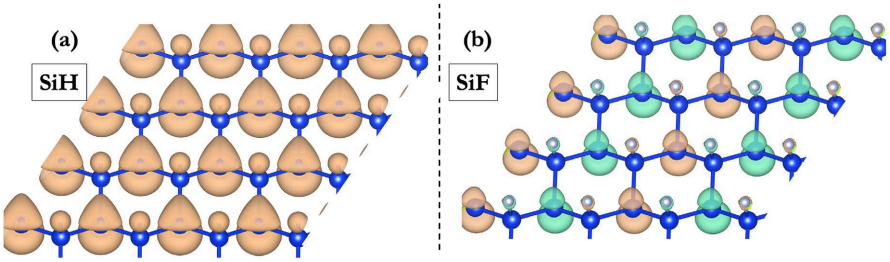

Figure 6. Spatial spin-density $\Delta\rho$ distributions for the $4 \times 4 \times 1$ supercells of the (a) half-hydrogenated and (b) half-fluorinated silicene configurations. The brown and green isosurfaces represent regions of positive (majority, spin-up) and negative (minority, spin-down) spin density, respectively. For both configurations, the plotted isovalue is set to 40% of the maximum spatial spin density.

To elucidate the microscopic origins of the induced magnetism and isolate the specific atomic orbital contributions, the spin-polarized projected density of states (PDOS) for both configurations is presented in Figure 7. For the half-hydrogenated system (Figure 7(a)), the PDOS reveals a pronounced asymmetry between the majority and minority spin channels, seamlessly corroborating its ferromagnetic ground state. The electronic states in the immediate vicinity of the Fermi level are overwhelmingly derived from the *p*-orbitals of the unpassivated silicon atoms, confirming that these specific orbitals act as the primary drivers of magnetism in the hydrogenated monolayer.

Conversely, the PDOS of the half-fluorinated configuration (Figure 7(b)) exhibits perfect symmetry between the spin-up and spin-down channels, reaffirming the macroscopic spin cancellation inherent to its antiferromagnetic state. No-

tably, the Fermi level is shifted into the valence band, consistent with the previously established semi-metallic character. The frontier states surrounding the Fermi energy are dictated primarily by the *p*-orbitals of the unpassivated silicon atoms, while the *p*-orbitals of the fluorine adatoms dominate the unoccupied states situated just above the Fermi level. This multi-orbital contribution demonstrates that the magnetic behavior in the half-fluorinated lattice emerges from the complex hybridization between the free silicon states and the highly electronegative fluorine adatoms.

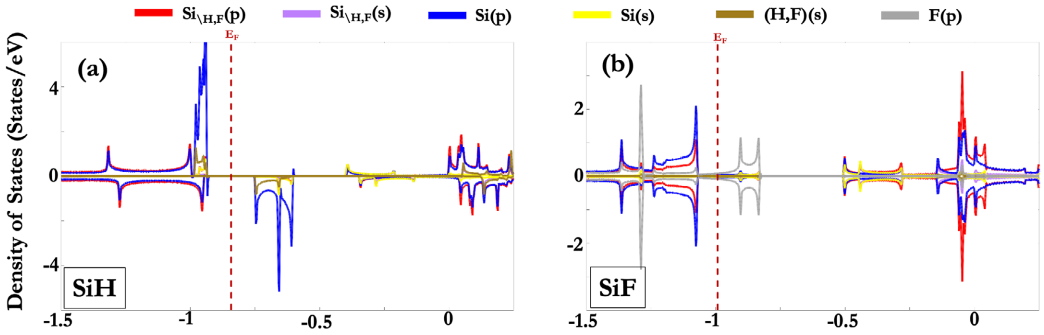

Figure 7. Spin-polarized projected density of states (PDOS) for the half-functionalized silicene configurations. (a) The half-hydrogenated system, illustrating the asymmetric spin distribution characteristic of its ferromagnetic ground state. (b) The half-fluorinated system, displaying a perfectly symmetric spin distribution indicative of its antiferromagnetic ground state.

Ultimately, the ability to engineer distinct electronic and magnetic ground states in silicene through targeted half-functionalization holds significant fundamental interest. Because silicene is inherently compatible with existing silicon infrastructure, demonstrating that adatom adsorption can tune the lattice between an antiferromagnetic semi-metal and a ferromagnetic semiconductor provides a valuable theoretical baseline for 2D magnetoelectronics. While the low Curie temperature (T_C = 30.6 K) of the hydrogenated system restricts potential spintronic applications strictly to cryogenic environments, this study confirms that chemical passivation is a highly effective, non-destructive mechanism to manipulate spin degrees of freedom in Dirac materials.

4. Conclusion

In conclusion, we have performed a comprehensive first-principles investigation into the phase engineering of silicene via half-functionalization with hydrogen and fluorine. Both configurations are demonstrated to be thermodynamically stable, exhibiting significant vertical charge transfer that generates strongly polarized, mixed ionic-covalent Si-adatom bonds without disrupting the purely covalent integrity of the basal Si-Si network. By explicitly breaking the intrinsic sublattice symmetry, half-adsorption dramatically transforms the zero-gap Dirac semi-metal into distinct, highly tunable electronic and magnetic phases. Specifically, half-hydrogenation yields an indirect-gap semiconductor with a ferromagnetic ground state,

driven predominantly by the localized *p*-orbitals of the unpassivated silicon atoms. In stark contrast, half-fluorination produces an antiferromagnetic semi-metal, where the magnetic behavior is governed by the collective contribution from both the unpassivated Si and the adatom F *p*-orbitals. These results highlight that adatom selection in half-functionalized lattices provides a precise mechanism for controlling macroscopic spin ordering and electronic topology. Consequently, this controlled, site-selective approach positions functionalized silicene as an exceptionally promising candidate for advanced spintronic device integration.

Data Availability Statement

The data that support the findings of this study are available upon reasonable request from the authors.

Acknowledgements

The authors gratefully acknowledge the "Université de Man (Côte d'Ivoire)" for providing technical support and access to computing facilities used for all the calculations.

Conflicts of Interest

The authors declare that they have no known competing financial interests or personal relationships that could have appeared to influence the work reported in this paper.

References

[1] Novoselov, K.S., Geim, A.K., Morozov, S.V., Jiang, D., Zhang, Y., Dubonos, S.V., *et al*. (2004) Electric Field Effect in Atomically Thin Carbon Films. *Science*, **306**, 666-669. https://doi.org/10.1126/science.1102896

[2] Nair, R.R., Blake, P., Grigorenko, A.N., Novoselov, K.S., Booth, T.J., Stauber, T., *et al*. (2008) Fine Structure Constant Defines Visual Transparency of Graphene. *Science*, **320**, 1308-1308. https://doi.org/10.1126/science.1156965

[3] Shao, Z., Ye, X., Yang, L. and Wang, C. (2013) First-Principles Calculation of Intrinsic Carrier Mobility of Silicene. *Journal of Applied Physics*, **114**, Article ID: 093712. https://doi.org/10.1063/1.4820526

[4] Ye, X., Shao, Z., Zhao, H., Yang, L. and Wang, C. (2014) Intrinsic Carrier Mobility of Germanene Is Larger than Graphene's: First-Principle Calculations. *RSC Advances*, **4**, 21216-21220. https://doi.org/10.1039/c4ra01802h

[5] Ezawa, M. (2015) Monolayer Topological Insulators: Silicene, Germanene, and Stanene. *Journal of the Physical Society of Japan*, **84**, Article ID: 121003. https://doi.org/10.7566/jpsj.84.121003

[6] Molle, A., Grazianetti, C., Tao, L., Taneja, D., Alam, M.H. and Akinwande, D. (2018) Silicene, Silicene Derivatives, and Their Device Applications. *Chemical Society Reviews*, **47**, 6370-6387. https://doi.org/10.1039/c8cs00338f

[7] Cahangirov, S., Topsakal, M., Aktürk, E., Şahin, H. and Ciraci, S. (2009) Two- and One-Dimensional Honeycomb Structures of Silicon and Germanium. *Physical Review Letters*, **102**, Article ID: 236804. https://doi.org/10.1103/physrevlett.102.236804

[8] Matetskiy, A.V., Barla, A., Moras, P., Carbone, C., Milotti, V., Brondin, C.A., *et al*. (2025) Germanene-Based Two-Dimensional Magnet with Tunable Properties. *ACS Nano*, **19**, 20863-20870. https://doi.org/10.1021/acsnano.5c03331

[9] Averyanov, D.V., Sokolov, I.S., Platunov, M.S., Wilhelm, F., Rogalev, A., Gargiani, P., *et al*. (2020) Competing Magnetic States in Silicene and Germanene 2D Ferromagnets. *Nano Research*, **13**, 3396-3402. https://doi.org/10.1007/s12274-020-3027-y

[10] Carpenter, J., Kim, H., Suarez, J., van der Zande, A. and Miljkovic, N. (2022) The Surface Energy of Hydrogenated and Fluorinated Graphene. *ACS Applied Materials & Interfaces*, **15**, 2429-2436.

[11] Houssa, M., Scalise, E., Sankaran, K., Pourtois, G., Afanas'ev, V.V. and Stesmans, A. (2011) Electronic Properties of Hydrogenated Silicene and Germanene. *Applied Physics Letters*, **98**, Article ID: 223107. https://doi.org/10.1063/1.3595682

[12] Wei, W. and Jacob, T. (2013) Strong Many-Body Effects in Silicene-Based Structures. *Physical Review B*, **88**, Article ID: 045203. https://doi.org/10.1103/physrevb.88.045203

[13] Singh, S.K., Srinivasan, S.G., Neek-Amal, M., Costamagna, S., van Duin, A.C.T. and Peeters, F.M. (2013) Thermal Properties of Fluorinated Graphene. *Physical Review B*, **87**, Article ID: 104114. https://doi.org/10.1103/physrevb.87.104114

[14] Wang, W., Olovsson, W. and Uhrberg, R.I.G. (2016) Band Structure of Hydrogenated Silicene on Ag(111): Evidence for Half-Silicane. *Physical Review B*, **93**, Article ID: 081406. https://doi.org/10.1103/physrevb.93.081406

[15] Hu, J.Q., Zhang, J.H., Wu, S.Q. and Zhu, Z.Z. (2015) Hybrid Functional Studies on the Optical and Electronic Properties of Graphane and Silicane. *Solid State Communications*, **209**, 59-65. https://doi.org/10.1016/j.ssc.2015.02.021

[16] Pontes, R.B., Mançano, R.R., da Silva, R., Cótica, L.F., Miwa, R.H. and Padilha, J.E. (2018) Electronic and Optical Properties of Hydrogenated Group-IV Multilayer Materials. *Physical Chemistry Chemical Physics*, **20**, 8112-8118. https://doi.org/10.1039/c7cp08471d

[17] Hohenberg, P. and Kohn, W. (1964) Inhomogeneous Electron Gas. *Physical Review*, **136**, B864-B871. https://doi.org/10.1103/physrev.136.b864

[18] Giannozzi, P., Baroni, S., Bonini, N., Calandra, M., Car, R., Cavazzoni, C., *et al*. (2009) Quantum Espresso: A Modular and Open-Source Software Project for Quantum Simulations of Materials. *Journal of Physics: Condensed Matter*, **21**, Article ID: 395502. https://doi.org/10.1088/0953-8984/21/39/395502

[19] Kohn, W. and Sham, L.J. (1965) Self-Consistent Equations Including Exchange and Correlation Effects. *Physical Review*, **140**, A1133-A1138. https://doi.org/10.1103/physrev.140.a1133

[20] Perdew, J.P., Burke, K. and Ernzerhof, M. (1996) Generalized Gradient Approximation Made Simple. *Physical Review Letters*, **77**, 3865-3868. https://doi.org/10.1103/physrevlett.77.3865

[21] Lee, K., Murray, É.D., Kong, L., Lundqvist, B.I. and Langreth, D.C. (2010) Higher-Accuracy Van Der Waals Density Functional. *Physical Review B*, **82**, Article ID: 081101. https://doi.org/10.1103/physrevb.82.081101

[22] Thonhauser, T., Cooper, V.R., Li, S., Puzder, A., Hyldgaard, P. and Langreth, D.C. (2007) Van Der Waals Density Functional: Self-Consistent Potential and the Nature of the Van Der Waals Bond. *Physical Review B*, **76**, Article ID: 125112. https://doi.org/10.1103/physrevb.76.125112

[23] Blöchl, P.E. (1994) Projector Augmented-Wave Method. *Physical Review B*, **50**,

17953-17979. https://doi.org/10.1103/physrevb.50.17953

[24] Leenaerts, O., Peelaers, H., Hernández-Nieves, A.D., Partoens, B. and Peeters, F.M. (2010) First-Principles Investigation of Graphene Fluoride and Graphane. *Physical Review B*, **82**, Article ID: 195436 https://doi.org/10.1103/physrevb.82.195436

[25] Masson, L. and Prévot, G. (2023) Epitaxial Growth and Structural Properties of Silicene and Other 2D Allotropes of Si. *Nanoscale Advances*, **5**, 1574-1599. https://doi.org/10.1039/d2na00808d

[26] Nguyen, D.K., Hoang, D. and Hoat, D.M. (2022) Exploring a Silicene Monolayer as a Promising Sensor Platform to Detect and Capture NO and CO Gas. *RSC Advances*, **12**, 9828-9835. https://doi.org/10.1039/d2ra00442a

[27] Allen, L.C. (1989) Electronegativity Is the Average One-Electron Energy of the Valence-Shell Electrons in Ground-State Free Atoms. *Journal of the American Chemical Society*, **111**, 9003-9014. https://doi.org/10.1021/ja00207a003

[28] Sanville, E., Kenny, S.D., Smith, R. and Henkelman, G. (2007) Improved Grid-Based Algorithm for Bader Charge Allocation. *Journal of Computational Chemistry*, **28**, 899-908. https://doi.org/10.1002/jcc.20575

[29] Liu, C., Jiang, H. and Yao, Y. (2011) Low-Energy Effective Hamiltonian Involving Spin-Orbit Coupling in Silicene and Two-Dimensional Germanium and Tin. *Physical Review B*, **84**, Article ID: 195430. https://doi.org/10.1103/physrevb.84.195430

[30] Bruhn, G., Davidson, E.R., Mayer, I. and Clark, A.E. (2006) Löwdin Population Analysis with and without Rotational Invariance. *International Journal of Quantum Chemistry*, **106**, 2065-2072. https://doi.org/10.1002/qua.20981